TMCO1 Is an ER Ca^{2+} Load-Activated Ca^{2+} Channel

Graphical Abstract

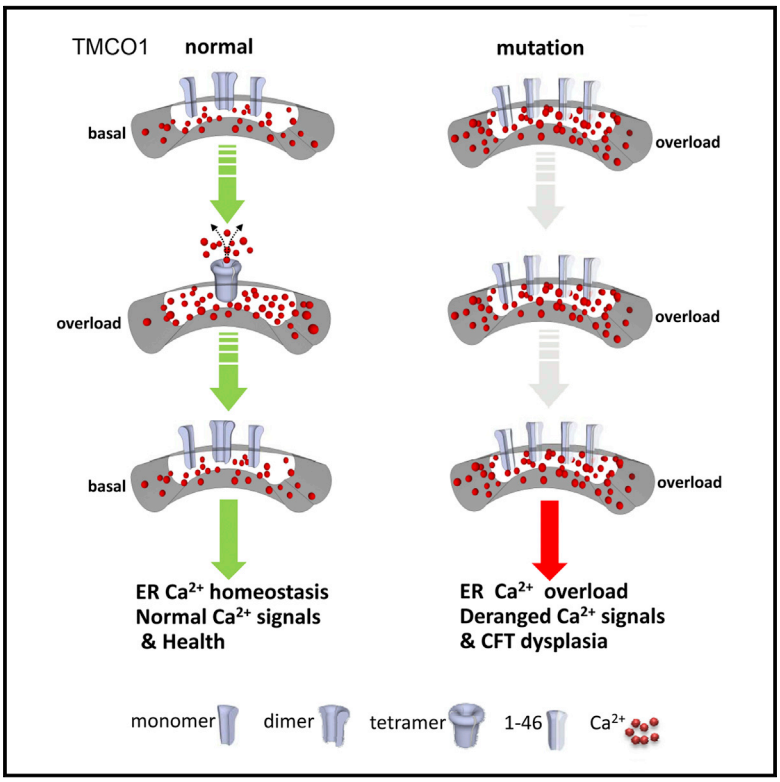

Highlights

- *TMCO1* gene encodes an evolutionarily conserved ER transmembrane-spanning protein
- Loss of TMCO1 causes overloading of ER Ca^{2+} store and mishandling of Ca^{2+} signaling
- TMCO1 assembles into a Ca^{2+} selective channel in response to ER Ca^{2+} overloading
- Ca^{2+} channel function of TMCO1 is disrupted by CFT dysplasia spectrum mutations

Authors

Qiao-Chu Wang, Qiaoxia Zheng, Haiyan Tan, ..., Quan Chen, Aimin Zhou, Tie-Shan Tang

In Brief

TMCO1 is an ER membrane channel that detects overfilling of calcium stores and restores calcium homeostasis, a function that is disrupted in human CFT dysplasia.

TMCO1 Is an ER Ca^{2+} Load-Activated Ca^{2+} Channel

Qiao-Chu Wang, Qiaoxia Zheng, Haiyan Tan, Bing Zhang, Xiaoling Li, Yuxiu Yang, Jie Yu, Yang Liu, Hao Chai, Xi Wang, Zhongshuai Sun, Jiu-Qiang Wang, Shu Zhu, Fengli Wang, Maojun Yang, Caixia Guo, Heng Wang Qingyin Zheng, Yang Li, Quan Chen, Aimin Zhou, and Tie-Shan Tang

SUMMARY

Maintaining homeostasis of Ca^{2+} stores in the endoplasmic reticulum (ER) is crucial for proper Ca^{2+} signaling and key cellular functions. The Ca^{2+}-release-activated Ca^{2+} (CRAC) channel is responsible for Ca^{2+} influx and refilling after store depletion, but how cells cope with excess Ca^{2+} when ER stores are overloaded is unclear. We show that TMCO1 is an ER transmembrane protein that actively prevents Ca^{2+} stores from overfilling, acting as what we term a "Ca^{2+} load-activated Ca^{2+} channel" or "CLAC" channel. TMCO1 undergoes reversible homotetramerization in response to ER Ca^{2+} overloading and disassembly upon Ca^{2+} depletion and forms a Ca^{2+}-selective ion channel on giant liposomes. TMCO1 knockout mice reproduce the main clinical features of human cerebrofaciothoracic (CFT) dysplasia spectrum, a developmental disorder linked to TMCO1 dysfunction, and exhibit severe mishandling of ER Ca^{2+} in cells. Our findings indicate that TMCO1 provides a protective mechanism to prevent overfilling of ER stores with Ca^{2+} ions.

INTRODUCTION

Calcium ion (Ca^{2+}) is a highly versatile intracellular signal that controls many different cellular functions such as contraction, secretion, memory formation, gene transcription, cell growth, and cell death (Berridge, 1993; Clapham, 2007). The endoplasmic reticulum (ER) is the main intracellular Ca^{2+} store. Ca^{2+} concentration in the ER ($[Ca^{2+}]_{ER}$) must be maintained in a steady state for proper Ca^{2+} signaling (Berridge et al., 2003; Clapham, 2007), and disarrangement of ER Ca^{2+} homeostasis has been implicated in many severe diseases (Bezprozvanny and Mattson, 2008; Sammels et al., 2010; Tu et al., 2006). Stimulation of cells with a variety of physiological stimuli leads to an inositol-1,4,5-trisphosphate (IP_3)-mediated Ca^{2+} release from ER and a depletion of Ca^{2+} stores (Berridge et al., 2003). Cells evolve a mechanism termed store-operated Ca^{2+} entry (SOCE) or capacitative Ca^{2+} entry (CCE) to refill the cell and ER Ca^{2+} stores (Cahalan, 2009; Lewis, 2007; Putney, 2009). It is known that Ca^{2+}-release-activated Ca^{2+} (CRAC) channels are responsible for the SOCE activity and Ca^{2+} store refilling after store depletion (Brandman et al., 2007; Feske et al., 2006; Liou et al., 2005; Luik et al., 2008; Park et al., 2009; Prakriya et al., 2006; Roos et al., 2005; Vig et al., 2006; Zhang et al., 2005). However, it remains unclear if there is a mechanism for ER to extrude the excess Ca^{2+} when the store gets overloaded.

Transmembrane and coiled-coil domains 1 (TMCO1)-defect syndrome is characterized by distinctive craniofacial dysmorphism, skeletal anomalies, mental retardation, ataxia, and many other clinical symptoms. A frameshift mutation in the *TMCO1* gene has been identified as the pathogenic cause for this autosomal-recessive syndrome in the isolated Old Order Amish of northeastern Ohio (Xin et al., 2010). The *TMCO1* gene encodes a protein predicted to be 188 amino acids, and its c.139_140delAG mutation is predicted to result in severe protein truncation (p.Ser47X) leading to a loss of protein function. Non-Amish cases with a nonsense mutation in the *TMCO1* gene (that results in a p.Arg87X truncation) have recently been reported (Alanay et al., 2014; Caglayan et al., 2013). TMCO1-defect syndrome, initially thought to represent a distinct disorder, belongs to the genetically heterogeneous cerebrofaciothoracic (CFT) dysplasia spectrum (Alanay et al., 2014).

The TMCO1 is a highly conserved protein among species (from slime-mold to human), implicating an evolutionarily conserved physiological function for TMCO1. However, the physiological function of TMCO1 is not known, nor the pathogenic mechanism of CFT dysplasia spectrum. Here, we provide biochemical and imaging, molecular and cellular,

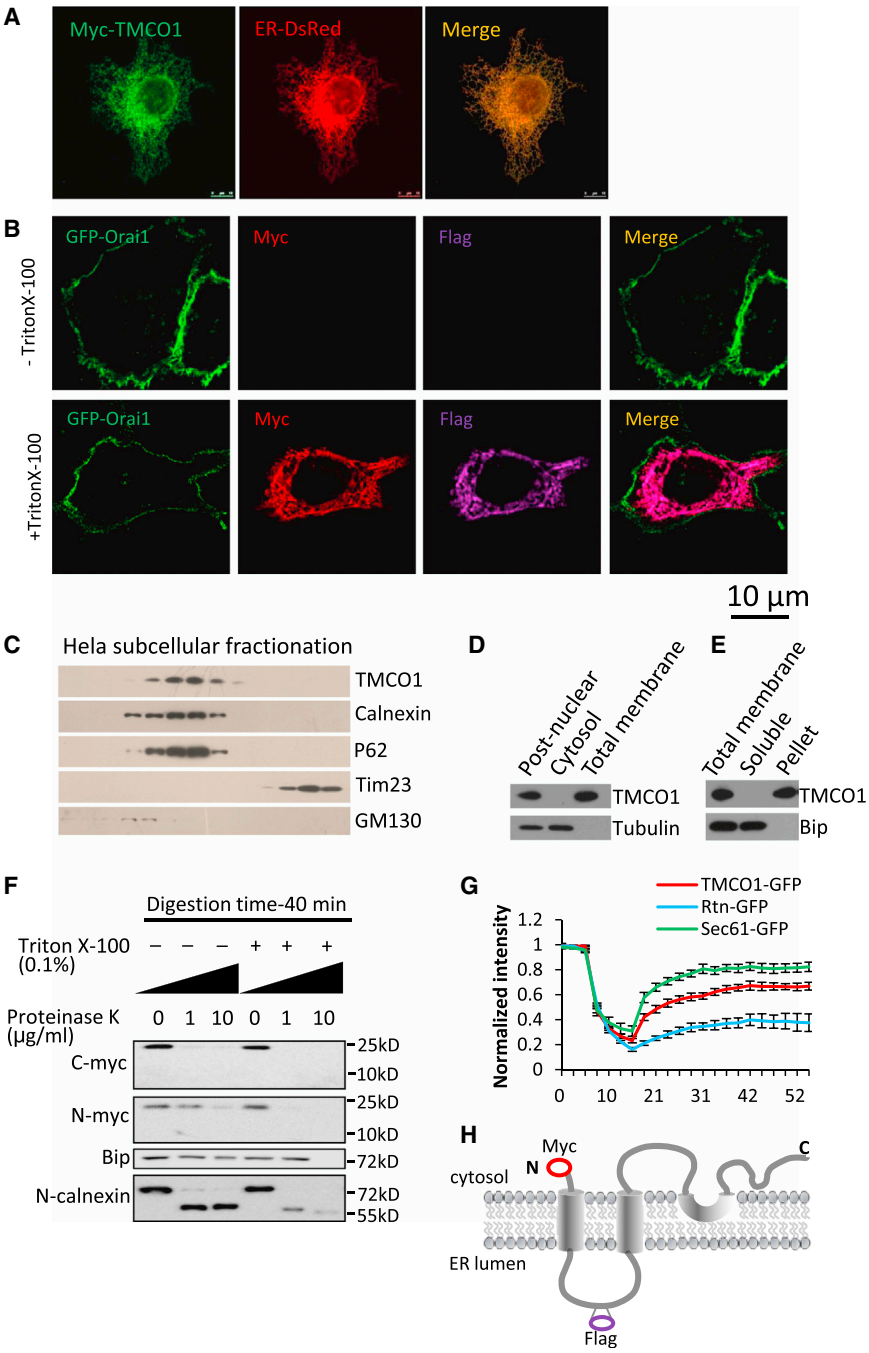

Figure 1. TMCO1 Is a Transmembrane-Spanning ER-Located Protein, with Both N and C Termini Stretched into the Cytoplasm

(A) HeLa cells expressing myc-tagged TMCO1 and endoplasmic reticulum (ER)-targeted DsRed (ER-DsRed) were fixed, permeabilized, and immunostained with anti-myc antibodies.

(B) Surface-labeling of Myc-Flag tagged TMCO1. Myc- and Flag-tag were located on the opposite side of the first transmembrane domain in TMCO1 (as shown in H). Immunostaining of Myc and Flag were carried out in intact (upper row, no Triton X) and permeabilized (lower row, with Triton X-100) cells. GFP-Orai1 was chosen as a marker of plasma membrane.

(C) Subcellular fractionation of HeLa cells. The post-nuclear supernatant (PNS) was fractionated on 30% Percoll and then subjected to western blotting with different antibodies. Calnexin and P62, ER proteins; Tim23, mitochondrial protein; GM130, Golgi protein.

(D) The TMCO1 presents in membrane fraction. Cytosol and total membrane from HeLa PNS were immunoblotted for TMCO1.

(E) TMCO1 is resistant to alkaline extraction. Both the pellet and the soluble fractions after alkaline extraction were immunoblotted for TMCO1 and Bip (ER intraluminal protein).

(F) Membrane topology experiments of TMCO1. PNS from HeLa cells expressing TMCO1 with either N-myc or C-myc tags were digested with proteinase K in the presence or absence of Triton X-100 followed by western blot analysis.

(G) Fluorescence recovery after photo-bleaching (FRAP) experiments of TMCO1-GFP. Rtn-4a and Sec61-beta are ER transmembrane proteins with low and high diffusible rates, respectively.

(H) Schematic representation of the membrane topology of TMCO1. Both N and C termini of TMCO1 were located in the cytoplasm.

See also Figure S1.

electrophysiological, and in vivo mouse model data demonstrating that TMCO1 is an ER transmembrane protein, which responses to ER luminal Ca^{2+} overloading by homotetramerization and functions as a Ca^{2+} overload-assembled Ca^{2+} release channel. This Ca^{2+} load-activated Ca^{2+} (CLAC) release channel constitutes a conserved general mechanism for cells to prevent ER Ca^{2+} store from overfilling and thus maintains a homeostasis in ER Ca^{2+} store. TMCO1-defect syndrome mutations fail to assemble the homotetramers leading to the CLAC channel disruption, which could be the underlying pathogenic mechanisms for human CFT dysplasia spectrum.

RESULTS

TMCO1 Is an ER Transmembrane-Spanning Protein

TMHMM sequence analysis of TMCO1 predicted two transmembrane segments (amino acids 9–31 for TM1 and amino acids 91–109 for TM2) and a hydrophobic stretch (amino acids 143-154) (Figures S1A and S1B). To examine the subcellular localization of TMCO1, myc-tagged TMCO1 was expressed in HeLa cells. Immunostaining of myc-TMCO1 showed perfect colocalization of myc-TMCO1 with ER tracker (Figure 1A), and the first transmembrane segment (TM1) of TMCO1 is essential for its ER localization (Figures S1C and S1D). Surface-labeling of two-side-tagged TMCO1 demonstrated that TMCO1 is not a plasma membrane

protein (Figure 1B). We next generated a polyclonal antibody against TMCO1 that is able to recognize the endogenous TMCO1 protein in immunoblotting analysis. Percoll gradient fractionation of the post-nuclear supernatant (PNS) revealed that endogenous TMCO1 is associated with the ER markers (calnexin, P62) but not the mitochondrial (Tim 23) or Golgi (GM130) marker (Figure 1C). TMCO1 was presented in the membrane fraction (Figure 1D) and was resistant to alkaline extraction (Figure 1E), demonstrating that TMCO1 is an ER transmembrane-spanning protein rather than a membrane-associated protein.

To determine the membrane topology of TMCO1, the PNS from HeLa cells expressing TMCO1 with either an N-myc or C-myc tag was digested with proteinase K in the presence or absence of Triton X-100 followed by western blot analysis. Bip, an ER luminal protein, was resistant to protease digestion unless the PNS was permeabilized by detergent, suggesting that the PNS membranes were intact (Figure 1F). In the same digestion conditions, both N-myc and C-myc tags were sensitive to protease digestion even in the absence of detergent, indicating that both N terminus and C terminus of TMCO1 are located in the cytoplasm (Figures 1F and 1H). Rtn-4a and Sec61-beta are known ER transmembrane proteins with low and high diffusion rates, respectively. Fluorescence recovery after photo-bleaching (FRAP) experiments revealed that the mobility of TMCO1 in the ER membrane was much higher than that of Rtn-4a and lower than that of Sec61-beta (Figure 1G), indicating that TMCO1 protein diffuses readily throughout the ER membrane.

Loss of TMCO1 Causes Supernormal Ca^{2+} Signaling and Overload of ER Ca^{2+} Store

ER is the main intracellular Ca^{2+} store and plays a central role in intracellular Ca^{2+} mobilization and dynamics (Berridge et al., 2003). To examine the potential role of TMCO1 in Ca^{2+} signaling system, we established TMCO1 knockdown (KD) cell lines. Knocking down TMCO1 did not change the morphology of the cell (Figures S2A and S2B) or the expression levels of $InsP_3Rs$ and Ca^{2+} pumps (sacro/ER Ca^{2+} ATPase [SERCA]) (Figure S2C). ATP, an agonist of PLC-$InsP_3$-coupled receptor, elicited several Ca^{2+} spikes in wild-type (WT) cells (Figure 2A), while KD cells exhibited a supernormal Ca^{2+} signaling in response to the same concentration of ATP: long-lasting Ca^{2+} spikes or a plateau-like Ca^{2+} transient (Figure 2B). Intracellular Ca^{2+} store is important for this supernormal Ca^{2+} signaling, as the supernormal Ca^{2+} signaling was still observed even in Ca^{2+}-free medium (Figures 2C, 2D, and S3A–S3C). Uncaged $InsP_3$ induced significantly higher amplitude of Ca^{2+} transient in KD cells as compared to WT cells (Figures 2E and 2F). Thapsigargin (TG), an inhibitor of SERCA Ca^{2+} pumps, induced more massive and longer-lasting Ca^{2+} signals in KD cells than in WT cells (Figures 2G and S3D–S3F). The size of TG-sensitive Ca^{2+} pools (the integrated areas under the TG-induced cytosolic Ca^{2+} curves) is 2.1-fold larger in KD cells than that in WT cells (Figure 2H). The supernormal Ca^{2+} signal and the increased size of TG-sensitive Ca^{2+} pools in KD cells were completely rescued by the expression of full-length TMCO1, but not by the Ser47X truncation (amino acids 1–46), the mutation in TMCO1-defect syndrome (Figures 2G, 2H, and S3A–S3F), indicating that loss of TMCO1 function leads to overfilled ER Ca^{2+} store in KD cells. The filling state of ER Ca^{2+} store was further confirmed by the ER-targeted cameleon (D1ER), a fluorescence resonance energy transfer (FRET)-based ER Ca^{2+} indicator (Palmer et al., 2004). KD cells showed a significantly higher ER Ca^{2+} concentration than WT cells (Figures 2I and 2J). Furthermore, expression of TMCO1 but not 1–46 truncation reduced the high level of ER Ca^{2+} in KD cells to the normal level (Figures 2I and 2J), confirming that loss of TMCO1 leads to overfilling of ER Ca^{2+} store. Interestingly, ectopic expression of TMCO1 in WT cells almost depleted ER Ca^{2+} stores (Figures S3G and S3H), and TMCO1 protein levels inversely correlated with the size of ER Ca^{2+} stores (Figures S3G and S3I), supporting an important role of TMCO1 in regulating the Ca^{2+} content in ER store. Notably, expression of *Caenorhabditis elegans* or zebrafish TMCO1 also reduced the high level of ER Ca^{2+} in KD cells to normal level, suggesting that the function of TMCO1 is evolutionarily conserved (Figures S3J and S3K). While TMCO1 knocking-down did not change the basal cytosolic Ca^{2+} levels in resting cells (Figures 2K and 2L), overexpression of TMCO1 in WT cells exhibited a dose-dependent elevation of basal cytosolic Ca^{2+} levels in both Ca^{2+}-containing (Figure 2M) and Ca^{2+}-free medium (Figure 2N), indicating that TMCO1 overexpression causes increased Ca^{2+} release from internal store.

Tetramerization of TMCO1 in Response to the Overload of ER Ca^{2+} Store

Overload of ER Ca^{2+} store caused by loss of TMCO1 prompted us to determine if TMCO1 acts as a Ca^{2+} channel across the ER membrane to prevent the Ca^{2+} store from overfilling. If this is the case, the functional TMCO1 channel must form an oligomeric complex comprising several TMCO1 subunits. To determine the TMCO1 stoichiometry, we applied similar biochemical techniques used previously to solve the stoichiometry of other channels. Co-immunoprecipitation results revealed that the full-length TMCO1, but not the 1–46 truncation, can co-assemble with full-length TMCO1 (Figure 3A). Treatment of HeLa cell lysates with increasing concentrations of two different lysine-reactive crosslinkers produced cross-linked species with sizes of ~40, ~80, and ~160 kDa on SDS-PAGE, consistent with the molecular masses of TMCO1 dimers, tetramers, and octamers, respectively (Figures 3B and 3C). The molecular mass of TMCO1 monomer is predicted ~21 kDa, and the size of cross-linked oligomeric species observed are integer multiples of the ~21 kDa TMCO1 monomer, indicating that the cross-linked products are integral homomultimers of the monomeric TMCO1 (Figures 3B and 3C).

Overload of ER Ca^{2+} stores may influence the TMCO1 stoichiometry. To analyze the effects of the Ca^{2+} filling state in the ER on TMCO1 stoichiometry, we performed chemical cross-linking experiments with HeLa cell lysates from the resting, Ca^{2+} store-depleted (TG + EGTA), and Ca^{2+} store-overloaded (8% ethanol) cells (Figure 3D). ER Ca^{2+} store depletion caused a slight decrease in the cross-linked tetramer intensity of TMCO1 (Figure 3D), while the ER Ca^{2+} store overload resulted in a 2.5-fold increase in the intensity of TMCO1 tetramers (Figure 3D), suggesting that the Ca^{2+} store overload induces tetramerization of TMCO1. To visualize the TMCO1 oligomerization in situ and in real-time, we expressed CFP- and YFP-tagged TMCO1 simultaneously in cells and analyzed the assembly of TMCO1 by FRET

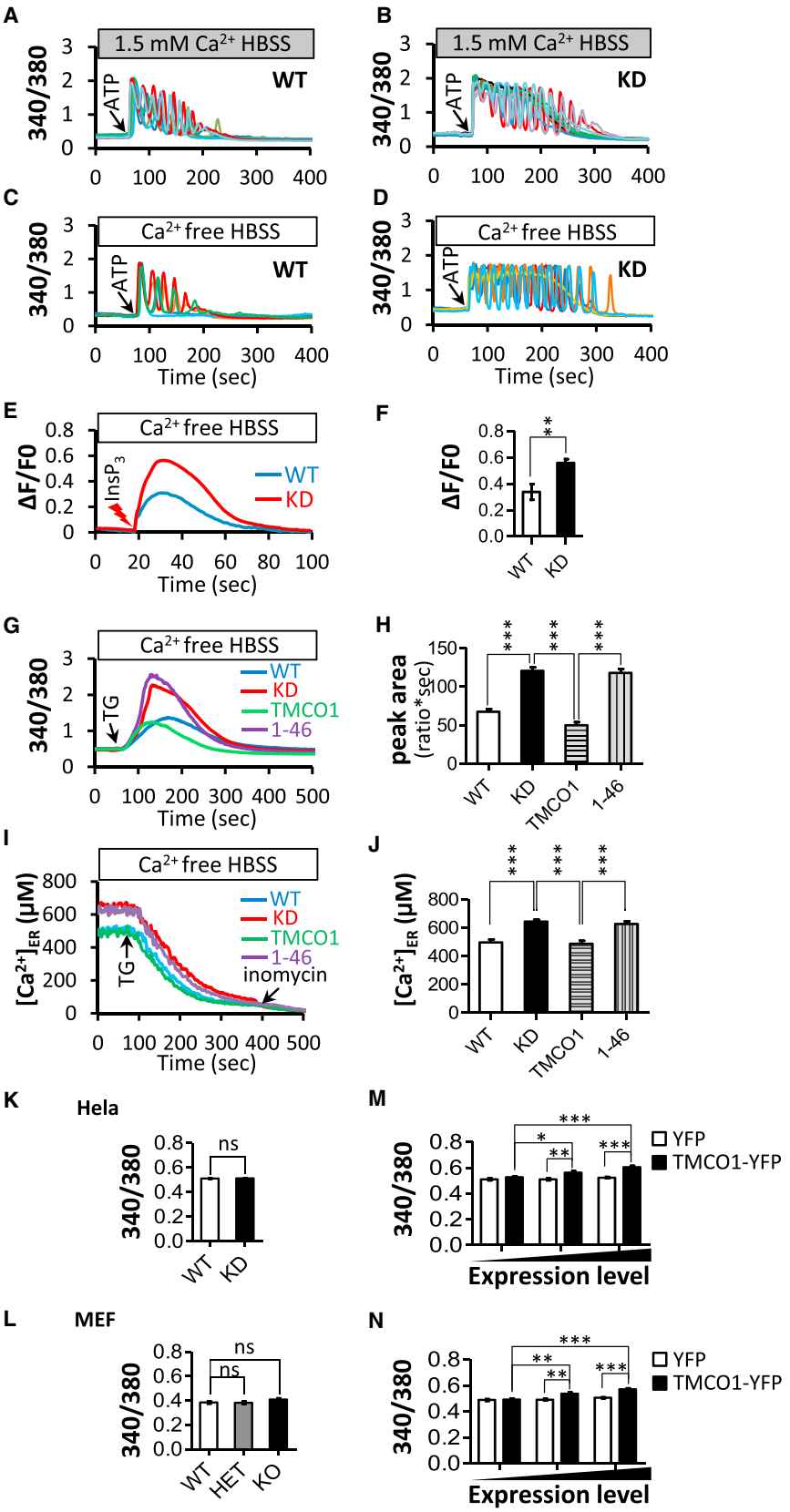

Figure 2. Loss of TMCO1 Leads to Supernormal Ca^{2+} Signaling and ER Ca^{2+} Overload

(A and B) ATP (1 μM)-evoked Ca^{2+} signaling in wild-type (WT) (A) and TMCO1 knockdown (KD) (B) cells in Ca^{2+}-containing medium. Fura-2 (340/380 ratio) was used to indicate the cytosolic Ca^{2+} concentration.

(C and D) ATP (1 μM)-evoked Ca^{2+} signaling in WT (C) and KD (D) cells in Ca^{2+}-free medium.

(E and F) Uncaged $InsP_3$ (2 μM)-triggered Ca^{2+} transients in WT cells (blue trace line, n = 17) and KD cells (red trace line, n = 17) in Ca^{2+}-free medium. Cytosolic Ca^{2+} concentration was represented by ΔF/F0 of Fluo-4. (F) Histogram shows the average amplitudes of $InsP_3$-triggered Ca^{2+} transients (mean ± SEM).

(G and H) Thapsigargin (TG)-triggered Ca^{2+} transients in WT (blue trace line, n = 23), KD (red trace line, n = 23), KD cells expressing TMCO1 (green trace line, n = 21), and KD cells expressing TMCO1 Ser47X truncation mutant (1–46, purple trace line, n = 22). (H) Histogram shows the average peak area of TG-triggered Ca^{2+} transients (mean ± SEM) in each group.

(I and J) ER Ca^{2+} levels were monitored by ER-targeted *cameleon* (*D1ER*) in WT (blue trace line, n = 80), KD (red trace line, n = 65), KD cells expressing TMCO1 (green trace line, n = 70), and KD cells expressing TMCO1 Ser47X truncation mutant (1–46, purple trace line, n = 55). The ER Ca^{2+} concentration was represented by μM. (J) Histogram shows the average ER Ca^{2+} levels in resting cells (mean ± SEM) in each group. Each trace line in (E), (G), and (I) is an average of Ca^{2+} responses from all cells in each group. All the experiments were repeated at least three times with similar results.

(K) Cytosolic Ca^{2+} levels in WT (n = 48) and KD (n = 49) HeLa cells.

(L) Cytosolic Ca^{2+} levels in WT (n = 23), HET (n = 27), and KO (n = 24) MEFs.

(M) Basal cytosolic Ca^{2+} levels in HeLa cells expressing TMCO1-YFP or YFP. Expression groups that cover the whole YFP fluorescence signals were created by grouping 20–50 cells (TMCO1-YFP, n = 150; control-YFP, n = 90). The average basal Ca^{2+} levels are plotted as a function of expression groups.

(N) Cells from (M) were changed to Ca^{2+}-free medium, and the average basal cytosolic Ca^{2+} levels were plotted to fluorescence ranges using the same data collected in (M). *p < 0.05, **p < 0.01, ***p < 0.001; ns, no significance.

See also Figures S2 and S3.

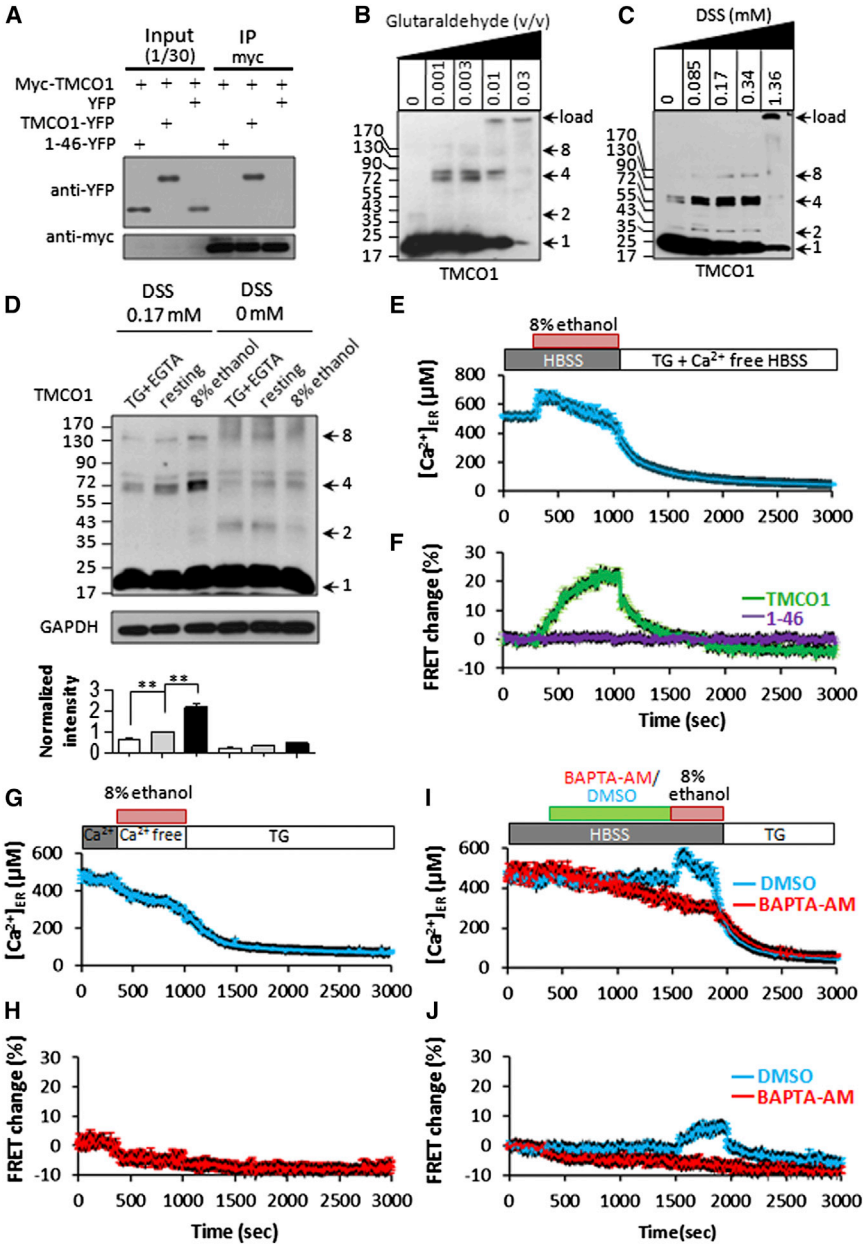

Figure 3. TMCO1 Undergoes Oligomerization and Forms Tetramers in Response to ER Ca^{2+} Overload

(A) Co-immunoprecipitation experiment (coIP) shows TMCO1 forms a complex with itself. The input lanes contained 1/30 of lysates used in coIP reactions. Representative of at least three independent experiments.

(B and C) Determination of the TMCO1 stoichiometry via chemical cross-linking. Increasing concentrations of glutaraldehyde (GA) (B) and disuccinimidyl suberate (DSS) (C) were used as indicated. Numbers represents the state of oligomerization: 1, monomer; 2, dimer; 4, tetramer; 8, octamer. Representative of at least three independent experiments.

(D) Similar experiments as (C) were performed on HeLa cell lysates prepared from resting cells, cells pre-treated with TG in Ca^{2+}-free medium (TG+EGTA), and cells pre-treated with 8% ethanol in Ca^{2+}-containing medium (8% ethanol). Representative of at least three independent experiments.

(E) D1ER indicated ER Ca^{2+} concentration manipulated by 8% ethanol in Ca^{2+} containing medium and by TG in Ca^{2+}-free medium (mean ± SEM, n = 9). Each trace line is shown in mean ± SEM.

(F) Time course of mean FRET ratio changes measured from individual cells expressing CFP- and YFP-tagged TMCO1 (green trace line, n = 16) or 1–46 (purple trace line, n = 6) after application of ethanol and TG. The FRET/CFP ratio before treatment was considered as basal, and FRET changes were represented in percentiles: 100 × $(R\text{-}R_{basal})/R_{basal}$. FRET increase means the assembly of TMCO1 and vice versa. Each trace line is shown in mean ± SEM.

(G and H) ER Ca^{2+} changes manipulated by 8% ethanol and TG in Ca^{2+} free medium (n = 21). FRET signal change of TMCO1 were shown in (H) (n = 25). Each trace line is shown in mean ± SEM.

(I) ER Ca^{2+} changes manipulated by 8% ethanol and TG in 40 μM of BAPTA-AM loaded cells (red trace line, n = 12). DMSO were used as control (blue trace line, n = 10). Each trace line is shown in mean ± SEM.

(J) FRET changes of TMCO1 were monitored according to the same procedure as above. Curve for control (DMSO, blue trace line, n = 9) and pre-treatment with BAPTA-AM (red trace line, n = 12) were shown. Each trace line is shown in mean ± SEM.

See also Figure S4.

method. TMCO1-CFP/YFP fusion proteins are functional if CFP or YFP is fused with the C terminus of TMCO1 (Figures S4C–S4F). Ethanol treatment induced an increase of ER Ca^{2+} concentration from a resting of ~500 μM to an overloaded state of ~650 μM. In contrast, TG depleted the ER Ca^{2+} effectively (Figure 3E). Accordingly, the FRET signal was increased ~20% upon ethanol-induced ER Ca^{2+} overload and reduced to ~−5% when ER Ca^{2+} was depleted (Figure 3F), indicating that the TMCO1 undergoes oligomerization in response to ER Ca^{2+} overload, and oligomerized TMCO1 (likely tetramers) rapidly disassembles when ER Ca^{2+} store returns to resting levels. 1–46 TMCO1 truncations lost the capability of oligomerization in response to 8% ethanol treatments (Figure 3F). Further data demonstrated that the effects of 8% ethanol on the changes of D1ER and FRET were $[Ca^{2+}]_{ER}$-dependent (Figures 3G–3J).

This reversible assembly/disassembly of TMCO1 at the single-molecule level in the native membrane environment was further determined by a photo-bleaching-step assay of TMCO1-GFP in TIRFM image. Continuous laser bleaching resulted in a stepwise decrement of GFP fluorescence at the diffraction-limited

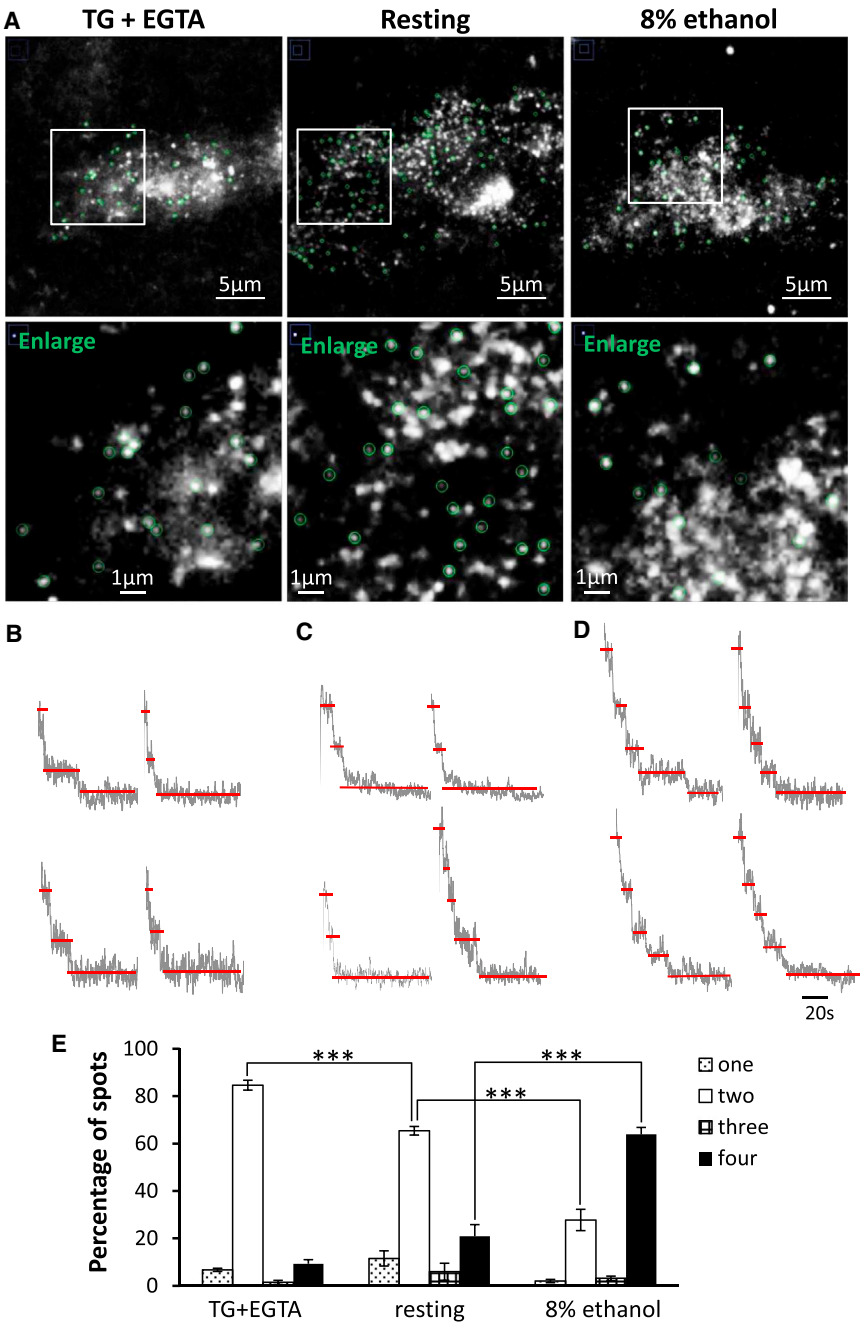

Figure 4. Tetramerization of TMCO1-GFP at the Single-Molecule Level in Response to the Overload of ER Ca^{2+} Store in Living Cells

(A) Representative TIRF images (first row) acquired before photo bleaching showed fluorescent spots (circled in green) sparsely distributed in the endoplasmic reticulum membrane of a HeLa cell expressing TMCO1-EGFP. Magnified views of boxed regions were also shown (second row). Laser photobleaching of GFP fluorescence is performed in TMCO1-GFP expressing HeLa cells (resting group, n = 5 cells, 226 spots; TG + EGTA group, n = 4 cells, 176 spots; 8% ethanol group, n = 4 cells, 306 spots).

(B–D) Representative examples of single-molecule laser bleaching traces recorded from HeLa cells. Two and four steps of laser bleaching traces were shown in (B), (C), and (D).

(E) Distribution of GFP-fluorescence bleaching steps with TIRF laser in living HeLa cells expressing TMCO1-EGFP. One to four steps of laser bleaching was shown in columns with dots, white, grid and black. Data are represented as mean ± SEM, ***p < 0.001.

fluorescent spots in TMCO1-GFP-expressing HeLa cells (Figures 4A–4D). The numbers of bleaching steps, ranging from one to a maximum of four, corresponding to the numbers of GFP molecules bleached at these spots (Figures 4B–4D). In resting HeLa cells, most of the spots (~65%) exhibited two steps to complete bleaching, and a small fraction (~20%) of these spots showed four bleaching steps (Figures 4C and 4E). ER Ca^{2+} overload resulted in a decrease of two-step bleaching spots (~28%) and an increase of four-step bleaching spots (~64%) (Figures 4D and 4E), whereas depletion of ER Ca^{2+} resulted in a completely opposite effect (Figures 4B and 4E). Therefore, TMCO1 is present in the ER membrane predominantly as dimers under resting conditions, and ER Ca^{2+} overload induces dimerization of TMCO1 dimers to form tetramers (Figure 4E), which could be functional as a putative Ca^{2+} channel across the ER membrane.

TMCO1 Forms a Ca^{2+} Permeable Channel across the ER Membrane

To determine whether TMCO1 is capable of forming a Ca^{2+}-permeable channel, we purified the TMCO1 proteins (Figure S5) and reconstituted them into liposomes. We successfully recorded the single channel currents with a conductance of 66 pS from liposomes incorporated with the wild-type TMCO1 protein (Figure 5A). In contrast, the disease mutant protein (Ser47X truncation) did not show any detectable channel currents (Figure 5B). The monovalent cation:anion selectivity was determined from reversal potentials measured in the presence of a 10-fold KCl gradient. TMCO1 exhibited an average reverse potential of −49.4 ± 2.1 mV, which gave rise to an estimated P_K/P_{Cl} of 24.6, indicating that TMCO1 is a cation selective channel (Figure 5D). The Ca^{2+} preference was then measured by the shift of reversal potential (ΔE_{rev}) when $CaCl_2$ was added to the bath solution (Figure 5D). Addition of 10 mM Ca^{2+} into bath solution caused the reversal potential of TMCO1 shifted from −49.4 ± 2.1 mV to 5.1 ± 0.2 mV (Figures 5A, 5D, and 5K; Table 1). This substantial shift of reversal potential suggested

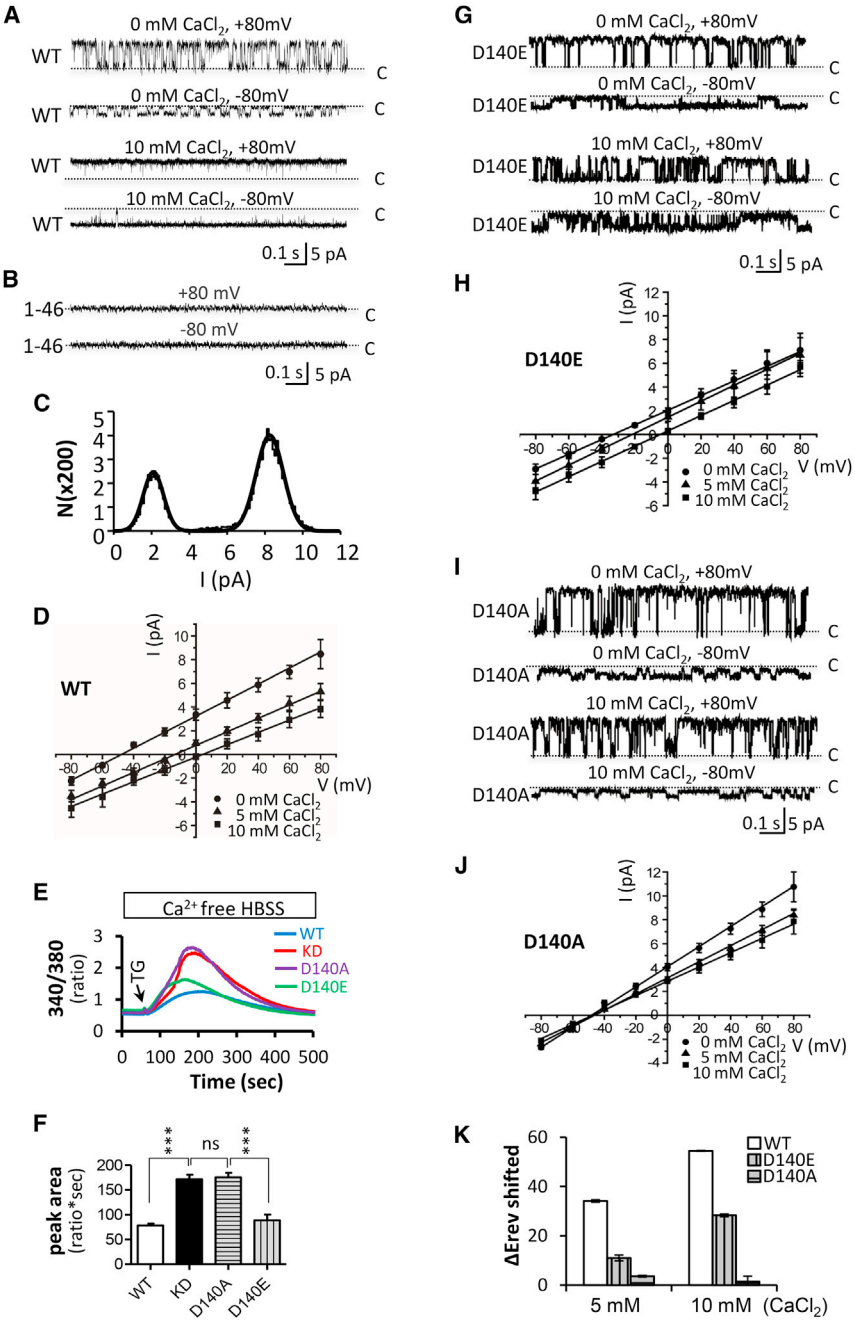

Figure 5. TMCO1 Protein Forms Ca^{2+}-Selective Ion Channels

(A) Single channel currents of TMCO1 were recorded from reconstituted giant liposome by the inside-out patch-clamping method. The traces recorded at 80 mV and −80 mV membrane voltages without or with 10 mM $CaCl_2$ in bath solutions were shown.

(B) TMCO1 disease mutant Ser47X truncation did not show any measurable currents.

(C) Histogram analysis of TMCO1 single channel current recorded at 80 mV as shown the top trace in (A), and two terms Gaussian fitting gave a high open probability (Po) of 0.68.

(D) The I-V plot by single channel conductance (pA) versus membrane voltage (mV). The black circle (●) represents the control solution (10:1 KCl gradient) without $CaCl_2$, and reversal potential of I-V is −49.4 ± 2.1 (mV), n = 5 patches. The black triangles (▲) represent the currents recorded after adding 5 mM $CaCl_2$ into the bath solution, with a reversal potential of −15.3 ± 0.5, n = 4 patches. The black squares (■) indicate the currents recorded after introducing 10 mM $CaCl_2$ into the bath solution, and the averaged reversal potential is 5.1 ± 0.2 mV, n = 4 patches.

(E) Thapsigargin (TG)-induced Ca^{2+} transients in WT (blue trace line, n = 29), KD (red trace line, n = 27), KD cells expressing TMCO1 mutant D140A (purple trace line, n = 31), and KD cells expressing TMCO1 mutant D140E (green trace line, n = 35).

(F) Histogram shows the average peak area of TG-triggered Ca^{2+} transients (mean ± SEM) in each group.

(G) Single channel current traces of TMCO1 mutant D140E recorded at 80 mV and −80 mV membrane voltages without or with 10 mM $CaCl_2$ in bath solution were shown.

(H) I-V curves of TMCO1 mutant D140E. Reversal potential shifted to right after addition of 5 mM or 10 mM $CaCl_2$ in bath solution.

(I) Single channel current traces of TMCO1 mutant D140A.

(J) I-V curves of TMCO1 mutant D140A. Note that there is no reversal potential shift after addition of 5 mM and 10 mM $CaCl_2$ in bath solution.

(K) Summarized shift of reversal potential of WT TMCO1, D140E mutant, and D140A mutant after adding 5 mM or 10 mM $CaCl_2$ in bath solution.

See also Figures S5 and S6.

that TMCO1 was obviously selective for Ca^{2+}. The conductance of TMCO1 reduced to 53.6 pS after adding 10 mM $CaCl_2$ in the bath solution (Table 1), which displayed a little inhibition of conductance, a typical phenomenon of Ca^{2+} permeation observed on the cyclic nucleotide-gated (CNG) ion channel (Almers and McCleskey, 1984; Frings et al., 1995). Many Ca^{2+} channels, such as CNG channels and IP_3 receptors (IP_3Rs), also conduct monovalent cations in the absence of divalent cations (Bezprozvanny and Ehrlich, 1994; Finn et al., 1997; Foskett et al., 2007).

To see if such conductance is present in vivo, we performed ER membrane patch clamp experiments. We made a tandem 4 × TMCO1 expressing plasmid and found that expression of tandem 4 × TMCO1 completely depleted the ER Ca^{2+} content, indicating that tandem 4 × TMCO1 is functional on ER (Figures S6A and S6B). ER patch-clamp recording of tandem 4 × TMCO1 expressing CHO cells mainly include two types of single channel: 12 out of 19 patches record small currents with 50.3 pS conductance (Figures S6C and S6E) and occasionally the large current ~400 pS, which is probably the currents of IP_3R or

Table 1. Characterizations of TMCO1 Channel and D140E, D140A Mutants

	Erev (mV)			Conductance (pS)		
	WT	D140E	D140A	WT	D140E	D140A
0 mM $CaCl_2$	−49.4 ± 2.1	−32.8 ± 0.6	−48.9 ± 1.3	66 ± 5.6	63.2 ± 9.6	81.7 ± 4.1
5 mM $CaCl_2$	−15.3 ± 0.5	−21.2 ± 1.2	−45.3 ± 0.4	56 ± 5.9	67.0 ± 17.3	67.1 ± 4.0
10 mM $CaCl_2$	5.1 ± 0.2	−3.9 ± 0.6	−47.5 ± 2.2	53.6 ± 6.3	62.0 ± 9.8	58.7 ± 5.5

The values of reversal potential (Erev, mV) and conductance of WT TMCO1, D140E, and D140A under asymmetric KCl solution (bath, 15 mM KCl; pipette, 150 mM KCl) with 0 mM, 5 mM, or 10 mM $CaCl_2$ in the bath solution were analyzed. The data are represented as the mean ± SEM, n = 4–7 patches.

RyR. The dominant currents of tandem 4 × TMCO1 has single channel conductance and open probability (Figure S6D, Po = 0.66) similar to the current of TMCO1 recorded from reconstituted giant liposome. In contrast, we were not able to record such single channel conductance in control CHO cells. Therefore, we have recorded the in vivo TMCO1 channel activity on ER membrane by ectopic expression of tandem 4 × TMCO1, supporting that TMCO1 is able to form a single channel conductance on ER membrane.

To further confirm that TMCO1 is a Ca^{2+} selective channel, we searched for the amino acids that potentially line the pore and interact with Ca^{2+}. We focused on the negatively charged residue aspartate at position 140 (D140) before the third hydrophobic stretch and changed it to either an alanine (D140A) or a glutamate (D140E) by site-directed mutagenesis. By functional evaluation of these mutations in Ca^{2+} imaging experiments, we found that charge-neutralizing mutant (D140A) lost the Ca^{2+} permeation function, whereas the charge-preserved mutant, D140E, still retained the ability to expel Ca^{2+} out of ER (Figures 5E and 5F).

These two mutants were then expressed, purified accordingly (Figure S5), and reconstituted into giant liposomes followed by patch-clamp experiments. Our electrophysiological results revealed that D140E mutation significantly reduced the shift of reversal potential (E_{rev} from −32.8 ± 0.6 mV to −3.9 ± 0.6 mV in the presence of 10 mM $CaCl_2$, Figures 5G, 5H, and 5K; Table 1), indicating that D140E attenuates the Ca^{2+} selectivity of TMCO1 channel. On the contrary, while D140A mutation showed a comparable K^+ preference (E_{rev} = −48.9 ± 1.3 mV; P_K/P_{Cl} ~22.4) as wild-type TMCO1, the reversal potential of D140A underwent almost no change after adding 10 mM Ca^{2+} into the bath solution (Figures 5I–5K; Table 1), revealing that substitution of D140 to an alanine eliminated the Ca^{2+} permeability of TMCO1 channel. Our results with point mutations therefore demonstrate that aspartate at position 140 is a key residue in the determination of Ca^{2+} preference and Ca^{2+} permeability of TMCO1, supporting the conclusion that TMCO1 can function as a Ca^{2+} channel across the ER membrane.

TMCO1 Knockout Mice Show a Delayed Osteogenesis, Mental Retardation, Ataxia, and Severe ER Ca^{2+} Mishandling

To examine the physiological role of TMCO1 in vivo, we generated *TMCO1* knockout (KO) mice (Figure S7A). Mutant mice lacking TMCO1 were viable. However, the birth rate of KO pups is only 8.9%, which is much less than theoretical probability of 25% from heterozygous matings, suggesting an antepartum death of KO fetuses (Figure 6A). *TMCO1*-KO pups exhibited a reduced body size (Figure S7B), low survival rate (Figure 6B), and delayed osteogenesis (Figures 6C and 6D). Micro-CT images of adult *TMCO1*-KO mice revealed the craniofacial dysmorphism such as open cranial sutures (Figure 6E; Movies S1 and S2), flattened faces with shorten nasal bones (Figure S7C), and skull anomalies (Figure S7D). Furthermore, magnetic resonance imaging (MRI) of *TMCO1*-KO mouse brain showed significantly enlarged brain ventricles (Figure 6F), suggesting a mental retardation in *TMCO1*-KO mice. Consistently, adult *TMCO1*-KO mice manifest the significant deficiency in spatial recognition memory in a Y-maze task assay (Figure 6G). The *TMCO1*-KO mice also showed a significant deficiency in motor coordination in rotarod assessments (Figure 6H). Thus, our *TMCO1*-KO mice recapitulate the main clinical features of human TMCO1 defect patients including high rate of miscarriage, developmental delay, craniofacial dysmorphism, enlarged brain ventricles, mental retardation, and unstable gait (Alanay et al., 2014; Xin et al., 2010), demonstrating that disruption of TMCO1 function in mice can cause similar symptoms to that of human CFT dysplasia spectrum. Notably, Ca^{2+} imaging results revealed the significant overload of ER Ca^{2+} in *TMCO1*-KO osteoblasts (Figures 6I, 6J, S7E, and S7F), illustrating the severe mishandling of ER Ca^{2+} after ablation of *TMCO1* in osteoblasts, which could be the underlying mechanism for the craniofacial anomalies in CFT dysplasia spectrum.

Taken together, we propose a model of how the ER Ca^{2+} store homeostasis is actively maintained by TMCO1. Our results show that *TMCO1*, a gene mutated in "TMCO1 defect syndrome/CFT dysplasia spectrum," encodes an evolutionarily conserved ER transmembrane-spanning protein. Overfilling of the ER with Ca^{2+} induces homotetramerization of TMCO1 to form an ER Ca^{2+} release channel. Ca^{2+} release via TMCO1 channels resets the ER Ca^{2+} concentration to resting level. TMCO1 homotetramers rapidly disassemble to terminate the channel activity when ER Ca^{2+} returns to resting level, thereby maintain a steady-state of ER Ca^{2+} levels in cells. Disease mutant TMCO1 proteins (such as the disease mutation Ser47X) failed to assemble a Ca^{2+} release channel and thus lose the function of preventing ER Ca^{2+} store from overload, leading to severe mishandling of ER Ca^{2+} and pathologies of human CFT dysplasia spectrum.

DISCUSSION

ER intraluminal Ca^{2+} concentration is crucial for initiation of proper Ca^{2+} signaling (Berridge et al., 2003; Clapham, 2007),

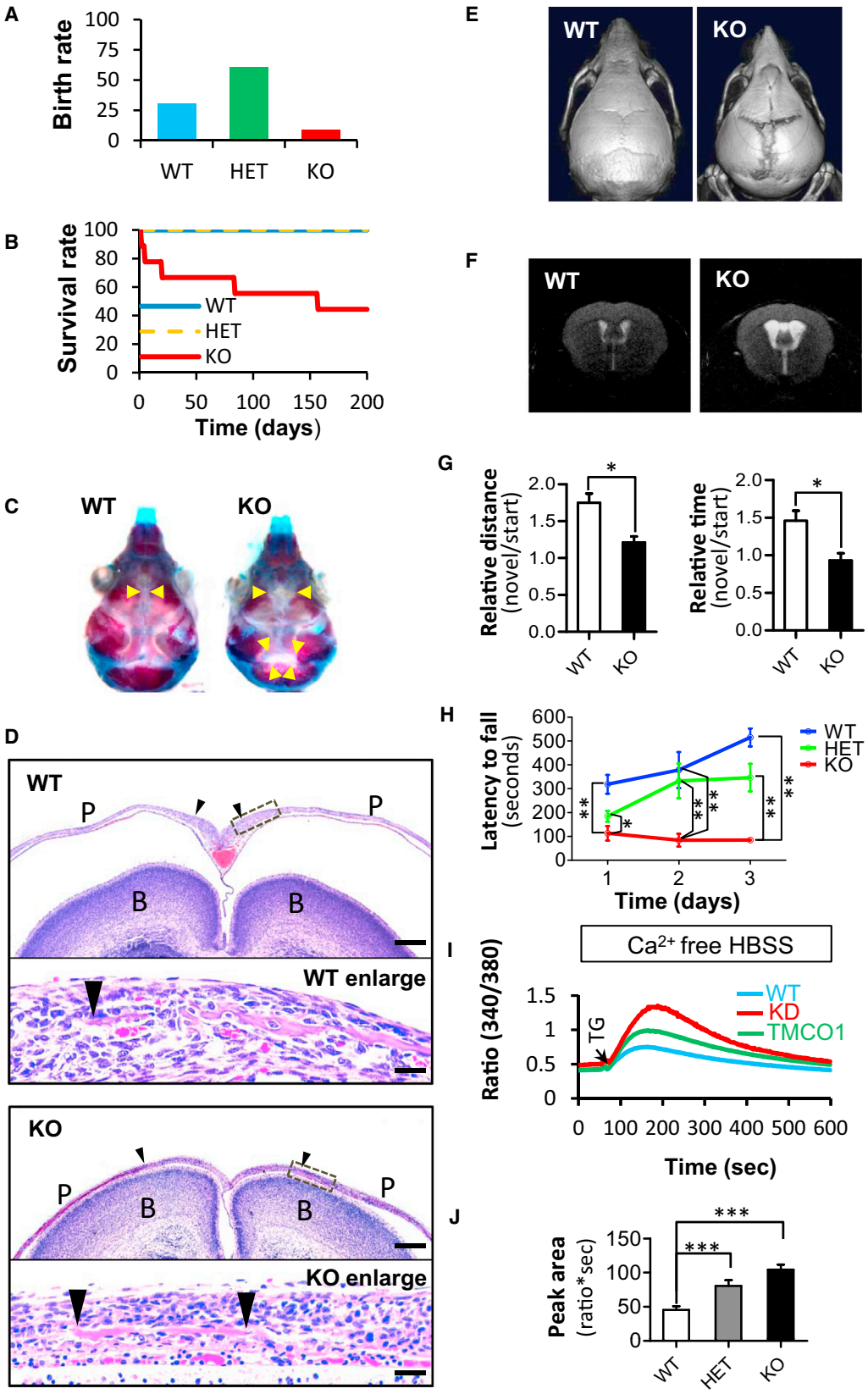

(legend on next page)

as well as correct protein folding and maturation (Austin, 2009; Xu et al., 2005). The content of ER Ca^{2+} store should be constantly monitored to maintain an ER Ca^{2+} homeostasis. STIM, an ER single-pass transmembrane protein, detects ER Ca^{2+} depletion (Liou et al., 2005; Roos et al., 2005; Stathopulos et al., 2008; Zhang et al., 2005), undergoes oligomerization (Baba et al., 2006; Liou et al., 2007; Wu et al., 2006), and directly binds to Orai (Muik et al., 2008; Park et al., 2009), causing the opening of the CRAC channel and initiation of Ca^{2+} entry to convey Ca^{2+} signals and to refill ER Ca^{2+} stores (Feske et al., 2006; Luik et al., 2008; Park et al., 2009; Prakriya et al., 2006; Roos et al., 2005; Vig et al., 2006; Yeromin et al., 2006; Yuan et al., 2009; Zhang et al., 2005). Here, we identify TMCO1 as an ER Ca^{2+} channel that detects ER Ca^{2+} overfilling and actively regulates ER Ca^{2+} content. TMCO1 is capable of sensing the ER Ca^{2+} overload status, assembling into a Ca^{2+} channel by homotetramerization, and thus releasing Ca^{2+} from ER store. Intriguingly, TMCO1 tetramers rapidly disassemble to terminate the Ca^{2+} channel activity when ER Ca^{2+} returns to resting levels. We believe that this reversible tetramerization/disassembly of TMCO1 in response to different ER Ca^{2+} levels constitutes an important and general mechanism for the maintenance of ER Ca^{2+} homeostasis. We name this channel as Ca^{2+} load-activated Ca^{2+} (CLAC) channel.

In resting cells, the steady-state ER Ca^{2+} level is determined by an equilibrium between SERCA-mediated Ca^{2+} uptake from the cytosol into the ER lumen and the passive leak of Ca^{2+} from ER into the cytosol (Berridge et al., 2003; Clapham, 2007). A number of candidates have been previously shown to play a role as Ca^{2+} passive leak channels, such as presenilins (Tu et al., 2006), BCL-2/IP_3R (Oakes et al., 2005), Bax inhibitor-1(Bultynck et al., 2012; Chae et al., 2004), and ryanodine receptor in cardiac cells (Jiang et al., 2005). Unlike the ''passive'' ER Ca^{2+} leak channels, TMCO1 is an ''active'' Ca^{2+} release channel that is assembled via homotetramerization in response to overfilled Ca^{2+} in the ER (Figures 3 and 4). The majority of TMCO1 do not assemble as homotetramers until the ER Ca^{2+} content reaches a critical high level, indicating that the main function of TMCO1 channel is to prevent ER store from overload of Ca^{2+}. Because ~20% of TMCO1 exist as homotetramers in resting cells (Figures 3F, 4C, and 4E), we consider that TMCO1 channel also accounts for a small proportion of basal ER Ca^{2+} leaking activity. This is further supported by the fact that knocking-down of TMCO1 leads to overload of ER Ca^{2+} store (Figures S3D–S3F), and overexpression of TMCO1 in WT cells almost depletes the ER Ca^{2+} store (Figures S3G–S3I).

Ca^{2+} influx system can also affect ER Ca^{2+} homeostasis. Capacitive Ca^{2+} entry through SOCE machinery is one of the major pathways for Ca^{2+} influx. SARAF, an ER located protein, has recently been discovered acting as an inhibitor of SOCE machinery to prevent excess Ca^{2+} refilling (Palty et al., 2012). Knocking-down SARAF can increase SOCE activity and thus causes ER Ca^{2+} overloading. We consider that SARAF and TMCO1, which act on plasma membrane SOCE machinery and ER membrane, respectively, work together to prevent ER Ca^{2+} overfilling and thus protect cells.

The *TMCO1* gene has highly conserved amino acid sequence among species, and complementation of the human *TMCO1* gene function can be achieved by expressing either *C. elegans* or zebrafish TMCO1 protein (Figures S3J and S3K), indicating that the TMCO1-mediated CLAC activity is an evolutionarily conserved mechanism for the homeostatic maintenance of ER Ca^{2+}. Given that homeostatic maintenance of ER Ca^{2+} is critical for proper Ca^{2+} signaling and cell functions (Berridge et al., 2003; Clapham, 2007), TMCO1 disease mutations-caused overload of ER Ca^{2+} store and supernormal intracellular Ca^{2+} signaling could be the underlying pathogenic mechanisms for human CFT dysplasia spectrum. Indeed, this has been confirmed by our *TMCO1*-knockout mouse model, which manifests severe mishandling of ER Ca^{2+} in disease-affected cells such as osteoblasts from newborn KO mouse skulls and a delayed osteogenesis.

Our *TMCO1*-KO mice successfully modeled the main clinical features of human TMCO1-defect syndrome such as developmental delay, craniofacial dysmorphism, enlarged brain ventricles and mental retardation, and unstable gait. We have

Figure 6. *TMCO1* Knockout Mice Show a Delayed Osteogenesis, Mental Retardation, Ataxia, and Severe ER Ca^{2+} Mishandling

(A) Percentage of each genotype at birth. WT, wild-type; HET, heterozygote; KO, *TMCO1*-knockout. Data are calculated from an overall 112 pups from heterozygous matings.

(B) Survival rate of each genotype. Data are calculated from an overall 112 pups from heterozygous matings.

(C) Alizarin Red S and Alcian Blue staining of the skulls of P4 mice. KO mouse skulls exhibit a significantly wider open frontier suture (between the two arrowheads) than its WT littermates.

(D) Histological analysis of P1 WT and KO mouse skulls. HE stainings show a significant wider gap between the left and right osteogenic fronts at the sagittal suture of KO pups (lower panels, pointed out with arrows) when compared with their WT littermates (upper panels, pointed out with arrows), and discontinuous osteoid deposition is seen at KO osteogenic fronts (lower enlarged panel, pointed out with arrows), revealing a delayed osteogenesis in P1 KO mice. Enlarged section was indicated with gray box in first and third panels. B, brain; P, parietal bone. Scale bars, 250 μm (first and third panels); 25 μm (second and fourth panels).

(E) Micro-CT of the skulls of 5-month-old WT and KO mice. KO skull shows obvious gaps along the midline interfrontal suture, transverse coronal and lambdoid sutures. Representative data from at least three KO mice are shown.

(F) Magnetic resonance imaging (MRI) of brains of 5-month-old mice show enlarged ventricles in KO mouse.

(G) Y-maze task assay of adult WT and KO mice. Relative distance walked (left panel) and relative time spent (right panel) of KO mice (black column, n = 6) in novel arm over start arm decrease significantly (*$p < 0.05$) than WT mice (white column, n = 10).

(H) Rotarod performance of adult WT and KO mice. An average latency to fall from the accelerating rotarod is shown for WT mice (blue, n = 10), HET mice (green, n = 8) and the KO mice (red, n = 6) in 3 consecutive days. For each group of mice, the results are shown as mean ± SEM. *$p < 0.05$; **$p < 0.01$.

(I and J) Overload of ER Ca^{2+} in primary osteoblasts cultured from *TMCO1*-KO mice. Curves represent TG-induced Ca^{2+} transients in WT (blue trace line, n = 34), KD (red trace line, n = 28), and HET (green line, n = 23) primary osteoblasts. (J) Histogram shows the average peak area of TG-triggered Ca^{2+} transients (mean ± SEM) in each group. Each curve in (I) is an average of Ca^{2+} responses from all cells in each group. ***$p < 0.001$.

See also Figure S7 and Movies S1 and S2.

previously described an autosomal-recessive syndrome, i.e., TMCO1-defect syndrome in the isolated Old Order Amish of northeastern Ohio (Xin et al., 2010). Recently, more Turkish origins of TMCO1-defect syndrome have been reported (Alanay et al., 2014; Caglayan et al., 2013). A combination of homozygosity mapping and whole-exome sequencing analysis of these patients of different origins have identified the pathogenic nonsense mutations in a single *TMCO1* gene (c.139_140delAG mutation, p.Ser47X truncation for Amish; c.259 C > T mutation, p.Arg87X truncation for Turkish). TMCO1-defect syndrome shares many features with cerebrofaciothoracic (CFT) dysplasia and could be considered to belong to the genetically heterogeneous CFT dysplasia spectrum (Alanay et al., 2014). The TMCO-deficient mouse model we created provides an important reagent for both molecular pathogenic mechanism studies and therapeutic target studies on CFT dysplasia spectrum in the future.

In summary, we have identified the TMCO1 as a conserved, important regulator of ER Ca^{2+} homeostasis. TMCO1 detects the ER Ca^{2+} loading status, undergoes reversible tetramerization/disassembly, and tightly regulates the Ca^{2+} content in ER store. This physiological function places TMCO1 as an important protective mechanism designed to prevent the overfilling of ER store with calcium ions.

EXPERIMENTAL PROCEDURES

Cell Culture and Transfection

HeLa, HEK293T, and COS7 cells were propagated and maintained as American Type Culture Collection (ATCC) recommended. Several TMCO1 knocking-down cell lines were generated by infection with small hairpin RNA (shRNA) lentiviral transduction particles produced by Sigma and maintained in DMEM containing puromycin with 10% FBS.

$[Ca^{2+}]$cyto and $[Ca^{2+}]_{ER}$ Measurements

Cytosolic Ca^{2+} concentration was measured by Fura-2 or Fluo4 as described previously (Tang et al., 2003), and $[Ca^{2+}]_{ER}$ measurements were done with D1ER probe as described before (Palmer et al., 2004). For more details, see the Supplemental Experimental Procedures.

Chemical Cross-linking

The following homobifunctional reagents were used for protein cross-linking: the lysine-reactive N-hydroxysuccimide esters DSS (water-insoluble, membrane permeable, spacer arm length 11.4 Å, dissolved in DMSO), and glutaraldehyde (GA, water-soluble, membrane permeable). Chemical cross-linking was accomplished as described previously with some modifications (Ramjeesingh et al., 1999). For more details, see the Supplemental Experimental Procedures.

Single-Molecule GFP Photobleaching

The single-molecule photobleaching experiments were performed as previously described (Ulbrich and Isacoff, 2007) with some modifications. TMCO1-GFP expressing in living HeLa cells was excited with a 488 nm laser through a TIRF objective (100×, oil, N.A. = 1.46; Leica DMI6000). For more details, see the Supplemental Experimental Procedures.

Preparation of Giant Liposomes and Electrical Recording

The purified wild-type TMCO1 and the mutants were reconstituted into lipid vesicles followed by dehydrate and hydrate processes. The giant liposome recording was performed by Axon200B patch-clamp system as previously described (Li et al., 2007). Asymmetrical solutions of 10:1 salt gradients (pipette solution, 150 mM KCl; bath solution, 15 mM KCl) were used. Currents were low-pass filtered at 1 or 10 kHz and sampled at 10 kHz or 100 kHz. Liquid junction potentials were calculated using JPCalc software (P. Barry, University of South Wales, Sydney, Australia).

Mice

TMCO1 knockout mice were generated by Shanghai Nanfang Laboratory for Model Organisms (Shanghai, China) using TALEN methods. TALENs targeting Exon1 of the TMCO1 gene was constructed by the Golden gate method. For more details and KO mouse-related assays, see the Supplemental Experimental Procedures. All animal experiments were reviewed and approved by the Institute of Zoology Institutional Animal Care and Use Committee and were conducted according to the committee's guidelines.

Statistical Analysis

Data are expressed as the mean ± SEM, and the statistical significance of differences between different groups was assessed using the t test or ANOVA with $p < 0.05$.

SUPPLEMENTAL INFORMATION

Supplemental Information includes Supplemental Experimental Procedures, seven figures, and two movies and can be found with this article online at http://dx.doi.org/10.1016/j.cell.2016.04.051.

AUTHOR CONTRIBUTIONS

Q.-C.W., Q.Z., H.T., and X.L. designed and performed cDNA constructs, cell biology, and biochemical experiments. Q.-C.W. performed Ca^{2+} imaging, FRET, single-molecule bleaching, and KO mice-related assays. B.Z., Y.Y., and H.C. performed electrophysiological experiments. J.Y. and Y. Liu performed the protein purifications. X.W. and Z.S. constructed the TMCO1-CFP/YFP/RFP and TMCO1 mutations. J.-Q.W. and S.Z. collaborated on Ca^{2+} imaging and FRET assays. F.W. collaborated on coIP and cross-linking experiments. M.Y. and C.G. provided advice and supervised the protein expression and purifications. H.W. and Q.Z. supervised the molecular biology experiments. Y. Li. supervised the electrophysiological experiments and analyzed the data. Q.C. supervised the cell biology experiments and analyzed the data. T.-S.T. and A.Z. conceived the study, provided advice and overall direction, and supervised project planning and execution. T.-S.T., Q.-C.W., and Y. Li. wrote the paper.

ACKNOWLEDGMENTS

We thank Yun Wang, Yang Zhang, and Wenjuan Xie for assistance in stable cell lines and constructs; Pingsheng Liu for help with cross-linking; Liangyi Chen for help with single-molecule bleaching; Junjie Hu for help with subcellular localization; Heping (Peace) Cheng for critical reading of the manuscript and helpful discussion; Paula L. Fischhaber for proofreading the manuscript; Roger Tsien for providing cameleon plasmids; Amy Palmer, Weiwei Shen, and Nicolas Demaurex for help with ER Ca^{2+} measurements. This work was supported by grants to T.-S.T. (National Basic Research Program of China 2012CB944702; NSFC 81371415, 91519324, 31570816, 31401151, and 81300982), A.Z. (awards from the Ohio Research Scholars Program and the Faculty Research and Development Program of Cleveland State University), Y. Li (2013CB91060101, 3137106601, 3117101101, and 2012ZX09301), M.Y. (2011CB910502, 2012CB911101, NSFC 31030020, and 31170679), and C.G. (2013CB945003, 31471331, and XDB14030302).

REFERENCES

Alanay, Y., Ergüner, B., Utine, E., Haçariz, O., Kiper, P.O., Taşkıran, E.Z., Perçin, F., Uz, E., Sağiroğlu, M.S., Yuksel, B., et al. (2014). TMCO1 deficiency

causes autosomal recessive cerebrofaciothoracic dysplasia. Am. J. Med. Genet. A. *164A*, 291–304.

Almers, W., and McCleskey, E.W. (1984). Non-selective conductance in calcium channels of frog muscle: calcium selectivity in a single-file pore. J. Physiol. *353*, 585–608.

Austin, R.C. (2009). The unfolded protein response in health and disease. Antioxid. Redox. Signal. *11*, 2279–2287.

Baba, Y., Hayashi, K., Fujii, Y., Mizushima, A., Watarai, H., Wakamori, M., Numaga, T., Mori, Y., Iino, M., Hikida, M., and Kurosaki, T. (2006). Coupling of STIM1 to store-operated Ca2+ entry through its constitutive and inducible movement in the endoplasmic reticulum. Proc. Natl. Acad. Sci. USA *103*, 16704–16709.

Berridge, M.J. (1993). Inositol trisphosphate and calcium signalling. Nature *361*, 315–325.

Berridge, M.J., Bootman, M.D., and Roderick, H.L. (2003). Calcium signalling: dynamics, homeostasis and remodelling. Nat. Rev. Mol. Cell Biol. *4*, 517–529.

Bezprozvanny, I., and Ehrlich, B.E. (1994). Inositol (1,4,5)-trisphosphate (InsP3)-gated Ca channels from cerebellum: conduction properties for divalent cations and regulation by intraluminal calcium. J. Gen. Physiol. *104*, 821–856.

Bezprozvanny, I., and Mattson, M.P. (2008). Neuronal calcium mishandling and the pathogenesis of Alzheimer's disease. Trends Neurosci. *31*, 454–463.

Brandman, O., Liou, J., Park, W.S., and Meyer, T. (2007). STIM2 is a feedback regulator that stabilizes basal cytosolic and endoplasmic reticulum Ca2+ levels. Cell *131*, 1327–1339.

Bultynck, G., Kiviluoto, S., Henke, N., Ivanova, H., Schneider, L., Rybalchenko, V., Luyten, T., Nuyts, K., De Borggraeve, W., Bezprozvanny, I., et al. (2012). The C terminus of Bax inhibitor-1 forms a Ca2+-permeable channel pore. J. Biol. Chem. *287*, 2544–2557.

Caglayan, A.O., Per, H., Akgumus, G., Gumus, H., Baranoski, J., Canpolat, M., Calik, M., Yikilmaz, A., Bilguvar, K., Kumandas, S., and Gunel, M. (2013). Whole-exome sequencing identified a patient with TMCO1 defect syndrome and expands the phenotic spectrum. Clin. Genet. *84*, 394–395.

Cahalan, M.D. (2009). STIMulating store-operated Ca(2+) entry. Nat. Cell Biol. *11*, 669–677.

Chae, H.J., Kim, H.R., Xu, C., Bailly-Maitre, B., Krajewska, M., Krajewski, S., Banares, S., Cui, J., Digicaylioglu, M., Ke, N., et al. (2004). BI-1 regulates an apoptosis pathway linked to endoplasmic reticulum stress. Mol. Cell *15*, 355–366.

Clapham, D.E. (2007). Calcium signaling. Cell *131*, 1047–1058.

Feske, S., Gwack, Y., Prakriya, M., Srikanth, S., Puppel, S.H., Tanasa, B., Hogan, P.G., Lewis, R.S., Daly, M., and Rao, A. (2006). A mutation in Orai1 causes immune deficiency by abrogating CRAC channel function. Nature *441*, 179–185.

Finn, J.T., Solessio, E.C., and Yau, K.W. (1997). A cGMP-gated cation channel in depolarizing photoreceptors of the lizard parietal eye. Nature *385*, 815–819.

Foskett, J.K., White, C., Cheung, K.H., and Mak, D.O. (2007). Inositol trisphosphate receptor Ca2+ release channels. Physiol. Rev. *87*, 593–658.

Frings, S., Seifert, R., Godde, M., and Kaupp, U.B. (1995). Profoundly different calcium permeation and blockage determine the specific function of distinct cyclic nucleotide-gated channels. Neuron *15*, 169–179.

Jiang, D., Wang, R., Xiao, B., Kong, H., Hunt, D.J., Choi, P., Zhang, L., and Chen, S.R. (2005). Enhanced store overload-induced Ca2+ release and channel sensitivity to luminal Ca2+ activation are common defects of RyR2 mutations linked to ventricular tachycardia and sudden death. Circ. Res. *97*, 1173–1181.

Lewis, R.S. (2007). The molecular choreography of a store-operated calcium channel. Nature *446*, 284–287.

Li, Y., Berke, I., Chen, L., and Jiang, Y. (2007). Gating and inward rectifying properties of the MthK K+ channel with and without the gating ring. J. Gen. Physiol. *129*, 109–120.

Liou, J., Kim, M.L., Heo, W.D., Jones, J.T., Myers, J.W., Ferrell, J.E., Jr., and Meyer, T. (2005). STIM is a Ca2+ sensor essential for Ca2+-store-depletion-triggered Ca2+ influx. Curr. Biol. *15*, 1235–1241.

Liou, J., Fivaz, M., Inoue, T., and Meyer, T. (2007). Live-cell imaging reveals sequential oligomerization and local plasma membrane targeting of stromal interaction molecule 1 after Ca2+ store depletion. Proc. Natl. Acad. Sci. USA *104*, 9301–9306.

Luik, R.M., Wang, B., Prakriya, M., Wu, M.M., and Lewis, R.S. (2008). Oligomerization of STIM1 couples ER calcium depletion to CRAC channel activation. Nature *454*, 538–542.

Muik, M., Frischauf, I., Derler, I., Fahrner, M., Bergsmann, J., Eder, P., Schindl, R., Hesch, C., Polzinger, B., Fritsch, R., et al. (2008). Dynamic coupling of the putative coiled-coil domain of ORAI1 with STIM1 mediates ORAI1 channel activation. J. Biol. Chem. *283*, 8014–8022.

Oakes, S.A., Scorrano, L., Opferman, J.T., Bassik, M.C., Nishino, M., Pozzan, T., and Korsmeyer, S.J. (2005). Proapoptotic BAX and BAK regulate the type 1 inositol trisphosphate receptor and calcium leak from the endoplasmic reticulum. Proc. Natl. Acad. Sci. USA *102*, 105–110.

Palmer, A.E., Jin, C., Reed, J.C., and Tsien, R.Y. (2004). Bcl-2-mediated alterations in endoplasmic reticulum Ca2+ analyzed with an improved genetically encoded fluorescent sensor. Proc. Natl. Acad. Sci. USA *101*, 17404–17409.

Palty, R., Raveh, A., Kaminsky, I., Meller, R., and Reuveny, E. (2012). SARAF inactivates the store operated calcium entry machinery to prevent excess calcium refilling. Cell *149*, 425–438.

Park, C.Y., Hoover, P.J., Mullins, F.M., Bachhawat, P., Covington, E.D., Raunser, S., Walz, T., Garcia, K.C., Dolmetsch, R.E., and Lewis, R.S. (2009). STIM1 clusters and activates CRAC channels via direct binding of a cytosolic domain to Orai1. Cell *136*, 876–890.

Prakriya, M., Feske, S., Gwack, Y., Srikanth, S., Rao, A., and Hogan, P.G. (2006). Orai1 is an essential pore subunit of the CRAC channel. Nature *443*, 230–233.

Putney, J.W. (2009). Capacitative calcium entry: from concept to molecules. Immunol. Rev. *231*, 10–22.

Ramjeesingh, M., Huan, L.J., Garami, E., and Bear, C.E. (1999). Novel method for evaluation of the oligomeric structure of membrane proteins. Biochem. J. *342*, 119–123.

Roos, J., DiGregorio, P.J., Yeromin, A.V., Ohlsen, K., Lioudyno, M., Zhang, S., Safrina, O., Kozak, J.A., Wagner, S.L., Cahalan, M.D., et al. (2005). STIM1, an essential and conserved component of store-operated Ca2+ channel function. J. Cell Biol. *169*, 435–445.

Sammels, E., Parys, J.B., Missiaen, L., De Smedt, H., and Bultynck, G. (2010). Intracellular Ca2+ storage in health and disease: a dynamic equilibrium. Cell Calcium *47*, 297–314.

Stathopulos, P.B., Zheng, L., Li, G.Y., Plevin, M.J., and Ikura, M. (2008). Structural and mechanistic insights into STIM1-mediated initiation of store-operated calcium entry. Cell *135*, 110–122.

Tang, T.S., Tu, H., Chan, E.Y., Maximov, A., Wang, Z., Wellington, C.L., Hayden, M.R., and Bezprozvanny, I. (2003). Huntingtin and huntingtin-associated protein 1 influence neuronal calcium signaling mediated by inositol-(1,4,5) triphosphate receptor type 1. Neuron *39*, 227–239.

Tu, H., Nelson, O., Bezprozvanny, A., Wang, Z., Lee, S.F., Hao, Y.H., Serneels, L., De Strooper, B., Yu, G., and Bezprozvanny, I. (2006). Presenilins form ER Ca2+ leak channels, a function disrupted by familial Alzheimer's disease-linked mutations. Cell *126*, 981–993.

Ulbrich, M.H., and Isacoff, E.Y. (2007). Subunit counting in membrane-bound proteins. Nat. Methods *4*, 319–321.

Vig, M., Peinelt, C., Beck, A., Koomoa, D.L., Rabah, D., Koblan-Huberson, M., Kraft, S., Turner, H., Fleig, A., Penner, R., and Kinet, J.P. (2006). CRACM1 is a plasma membrane protein essential for store-operated Ca2+ entry. Science *312*, 1220–1223.

Wu, M.M., Buchanan, J., Luik, R.M., and Lewis, R.S. (2006). Ca2+ store depletion causes STIM1 to accumulate in ER regions closely associated with the plasma membrane. J. Cell Biol. *174*, 803–813.

Xin, B., Puffenberger, E.G., Turben, S., Tan, H., Zhou, A., and Wang, H. (2010). Homozygous frameshift mutation in TMCO1 causes a syndrome with craniofacial dysmorphism, skeletal anomalies, and mental retardation. Proc. Natl. Acad. Sci. USA *107*, 258–263.

Xu, C., Bailly-Maitre, B., and Reed, J.C. (2005). Endoplasmic reticulum stress: cell life and death decisions. J. Clin. Invest. *115*, 2656–2664.

Yeromin, A.V., Zhang, S.L., Jiang, W., Yu, Y., Safrina, O., and Cahalan, M.D. (2006). Molecular identification of the CRAC channel by altered ion selectivity in a mutant of Orai. Nature *443*, 226–229.

Yuan, J.P., Zeng, W., Dorwart, M.R., Choi, Y.J., Worley, P.F., and Muallem, S. (2009). SOAR and the polybasic STIM1 domains gate and regulate Orai channels. Nat. Cell Biol. *11*, 337–343.

Zhang, S.L., Yu, Y., Roos, J., Kozak, J.A., Deerinck, T.J., Ellisman, M.H., Stauderman, K.A., and Cahalan, M.D. (2005). STIM1 is a Ca2+ sensor that activates CRAC channels and migrates from the Ca2+ store to the plasma membrane. Nature *437*, 902–905.